

A new stable boundary-layer mixing scheme and its impact on the simulated East Asian summer monsoon

Song-You Hong

Department of Atmospheric Sciences and Global Environment, Yonsei University, Seoul, South Korea

*Correspondence to: Song-You Hong, Department of Atmospheric Sciences, Yonsei University, Seoul, 120-749, Korea.
E-mail: shong@yonsei.ac.kr

This paper investigates the impact of **stable boundary-layer (SBL) mixing** in a vertical diffusion package on the simulated climatology in a regional model. In contrast to previous studies, we focus on the sensitivity of the simulated climatology to the representation of SBL processes in the modelled atmosphere, paying particular attention to precipitation and associated large-scale patterns. The new SBL scheme, based on the bulk Richardson number between the surface layer and the top of the boundary layer and implemented in the Yonsei University (YSU) boundary-layer scheme, was evaluated against the local scheme in which the mixing coefficient is a function of the local Richardson number at a given model level.

A statistical evaluation of a series of short-range forecast confirms that the boundary-layer structure is closer to the radiosonde observation when the new SBL scheme is used. In a regional climate framework, the results with the new SBL scheme in July 2006 demonstrate that modulating the subcloud structure with enhanced vertical mixing improves the simulated monsoon climatology by displacing the monsoonal precipitation southwards. Together with the local effects of the enhanced SBL mixing that warms and dries the boundary layer, the dynamical feedbacks accompanying strengthened moisture convergence results in enhanced precipitation towards what was observed. A ten-member ensemble of three-month June–July–August simulations for 1999–2008 shows that the revised SBL scheme improves the temperature and moisture profiles in the lower troposphere as well as the precipitation climatology. The interannual variation of seasonal precipitation is more realistic over both land and oceans. Copyright © 2010 Royal Meteorological Society

Key Words: stable boundary layer; planetary boundary layer; precipitation interaction; PBL scheme

Received 1 November 2009; Revised 20 May 2010; Accepted 26 May 2010; Published online in Wiley Online Library 26 August 2010

Citation: Hong S-Y. 2010. A new stable boundary-layer mixing scheme and its impact on the simulated East Asian summer monsoon. *Q. J. R. Meteorol. Soc.* **136**: 1481–1496. DOI:10.1002/qj.665

1. Introduction

Hong and Pan (1996) showed that a slight change of parameters in boundary-layer (BL) formalism could significantly affect both the distribution and the amount of rainfall forecast in a global forecast system. Thus it is clear that the BL scheme is a sensitive factor that is particularly related to precipitation physics in both global short- and

medium-range forecast models and mesoscale models. In the global forecast model area, Basu *et al.* (2002) demonstrated that BL processes play a critical role in the simulation of a precipitating monsoon system over India by affecting the lower-tropospheric structure over the oceans. In the mesoscale model area, Bright and Mullen (2002) examined the impact of the BL scheme in predicting summer monsoon circulations over the southwestern United States, showing

that the BL scheme determines the convectively available potential energy (CAPE) to trigger moist convection. BL processes in the numerical model also have a significant influence on simulated hurricane intensity. For example, Braun and Tao (2000) showed that the intensity of hurricane Bob (1991) was closely related to the ratio of exchange coefficients of enthalpy and momentum in a mesoscale model. Further studies of Davis and Bosart (2002) and Li and Pu (2008) confirmed the importance of the model BL scheme to the hurricane intensity forecast.

In seasonal prediction and climate models, a few studies have been carried out on the impact of the BL parametrization scheme. Martin *et al.* (2000), which showed that the BL and cloud structure in the semi-permanent stratocumulus regions over the eastern subtropical oceans improved noticeably due to a change in the BL scheme. Also, Byun and Hong (2004) demonstrated that a more realistic treatment of BL structure in a general circulation model (GCM) improved the tropical precipitation and its anomalies in response to the sea surface temperature (SST) anomalies. Terra *et al.* (2004) demonstrated the improvement of simulated tropical precipitation by applying subgrid-scale orography information in the simulation of BL clouds. Shin and Ha (2007) also showed that realistic treatment of the BL improves the simulated climatology in a GCM, especially over the western Pacific and East Asia. In a regional climate area forced by the analysis data, Cha *et al.* (2008) demonstrated the importance of the BL processes in reproducing the summer monsoon circulation over East Asia.

The studies mentioned above can be categorized as sensitivity studies of the predicted precipitation and related large-scale changes to different BL schemes. The overall conclusion is that the non-local scheme based on Troen and Mahrt (1986) has been applied successfully, with further generalization and reformulation, to GCMs and to numerical weather prediction models (Holtslag and Boville, 1993; Hong and Pan, 1996; Hong *et al.*, 2006, hereafter HDN06). This kind of non-local scheme is preferable because, compared with the local- K approach through the inclusion of countergradient flux terms, it enables realistic development of a well-mixed layer. In contrast to the daytime unstable counterpart, the progress in understanding turbulence in the nocturnal stable BL has been slow (Mahrt *et al.*, 1999), and its parametrization in numerical models has not been well established (Beare *et al.*, 2006).

The Yonsei University (YSU) vertical diffusion package (HND06), which is a revised vertical diffusion package over the medium-range forecast (MRF) BL (Hong and Pan, 1996) has been extensively applied to weather prediction and climate studies since its addition to the Weather Research and Forecasting model (WRF; Skamarock *et al.*, 2008). Meanwhile, Kim *et al.* (2006) reported that the YSU BL scheme tends to mix too little over the cold oceans, although overall this scheme outperforms the Mellor–Yamada type scheme (Janjić, 1990). It is reported that the YSU BL scheme produces a too-low nocturnal BL height over the continental valley in New Mexico (F. Zhang 2006, personal communication), in that the observed PBL height is as high as 500 m in observations, whereas the corresponding values from the YSU scheme stays at the height of the lowest model level. One may argue that the tendency of the PBL height to remain at the lowest model level may be partly related to poor vertical resolution in NWP models. However, we

presume that these behaviours are regarded as mainly due to a deficiency in SBL mixing in the version of the YSU PBL, as of July 2007. This is consistent with the fact that the BL height in a stable regime is not systematically low in other PBL schemes in WRF. In the HND06 algorithm, the local- K profile method whose vertical mixing is determined by a local stability at a given level is applied to all the model levels above the mixed layer.

For these reasons, a revised SBL mixing algorithm has been devised for the YSU vertical diffusion package. The revised SBL mixing computes the exchange coefficients with a parabolic function with height as in the mixed layer, in which the top of the SBL is determined by the bulk Richardson number, Ri , following the study of Vickers and Mahrt (2004). This new SBL scheme is tested on the platform of a regional climate simulation. Unlike the previous BL sensitivity studies focusing on the effects of convective boundary layer (CBL) turbulence representation on the simulated results, this study focuses on the SBL structure and associated simulated precipitation. To the author's knowledge, there is no previous study on the role of SBL mixing and its effects on simulated climatology. Note that some previous parametrization studies on SBL development (e.g. Lee *et al.*, 2006; Steeneveld *et al.*, 2008) have been confined to the nocturnal SBL structure, rather than the impact on the resulting precipitation and associated large-scale circulation.

The objective of this study is to investigate the role of SBL mixing on the monsoonal circulations over East Asia. A short-range simulation for one month is designed to investigate the immediate effect of the SBL mixing on the PBL structure. The interaction between the SBL mixing and precipitation processes embedded within the large-scale circulations is examined in a regional climate testbed for July 2006. This was a major summer monsoonal precipitation period in Korea and Japan. The 10-year June–August (JJA) simulations from 1999 to 2008 are designed to evaluate the revised SBL processes for the simulated monsoonal circulations over East Asia. The following section provides a description of the revised SBL scheme implemented in the YSU scheme. Details on the experimental approach, including a description of the model and data used, are presented in section 3, and their results are discussed in section 4. This paper ends with concluding remarks in the final section.

2. Implementation of a revised SBL scheme in the YSU BL package

The YSU scheme is a modified K -theory, with an additional countergradient term that incorporates the contribution of large-scale eddies to the total flux. The turbulence diffusion equations for prognostic variables C (zonal wind u , meridional wind v , potential temperature θ , specific humidity for water vapour q , cloud water mixing ratio q_c , cloud ice mixing ratio q_i) can be expressed by

$$\frac{\partial C}{\partial t} = \frac{\partial}{\partial z} \left\{ K_c \left(\frac{\partial C}{\partial z} - \gamma_c \right) - \overline{(w'c')}_h \left(\frac{z}{h} \right)^3 \right\}, \quad (1)$$

where K_c is the eddy diffusivity coefficient and γ_c is a correction to the local gradient which incorporates the contribution of the large-scale eddies to the total flux. Here $\overline{(w'c')}_h$ is the flux at the inversion layer. The BL height h

is defined as the level in which minimum flux exists at the inversion level. The YSU scheme is briefly presented here to help to understand the model results. A complete description of the YSU scheme is given in HND06, together with an investigation study on the interaction between the BL and precipitation physics. A theoretical development of the explicit entrainment processes algorithm in the YSU scheme is given in Noh *et al.* (2003).

2.1. Mixed-layer diffusion

The momentum diffusivity coefficient is formulated as

$$K_{zm} = kw_s z \left(1 - \frac{z}{h}\right)^p, \tag{2}$$

where p is the profile shape exponent taken to be 2, k is the von Kármán constant ($= 0.4$), z is the height from the surface and h is the height of the PBL. The mixed-layer velocity-scale is represented as

$$w_s = \left(u_*^3 + \frac{8kw_{*b}^3 z}{h}\right)^{1/3}, \tag{3}$$

where u_* is the surface frictional velocity-scale, and the convective velocity-scale for moist air is

$$w_{*b} = \left\{ \frac{g}{\theta_{va}} \overline{(w'\theta'_v)_0} h \right\}^{1/3}.$$

The countergradient term for θ and momentum is given by

$$\gamma_c = b \frac{\overline{(w'c')_0}}{w_{s0}}, \tag{4}$$

where $\overline{(w'c')_0}$ is the corresponding surface flux for θ , u , and v , and b is a coefficient of proportionality. The mixed-layer velocity-scale w_{s0} in (4) is defined as the velocity at $z = 0.5 h$ in (3). The eddy diffusivity for temperature and moisture K_T is computed from K_m in (2) by using the relationship of the Prandtl number.

The flux at the inversion layer for scalars θ and q , and vector quantities u and v , is proportional to the jump of each variable at the inversion layer:

$$\overline{(w'c')_h} = w_e \Delta c|_h, \tag{5}$$

where w_e is the entrainment rate at the inversion layer.

The BL height is calculated as

$$h = Ri_{b,cr} \frac{\theta_{va} |U(h)|^2}{g \{\theta_v(h) - \theta_s\}}, \tag{6}$$

where $Ri_{b,cr}$ is the critical bulk Richardson number ($= 0$), $U(h)$ is the horizontal wind speed at h , θ_{va} is the virtual potential temperature at the lowest model level, $\theta_v(h)$ is the virtual potential temperature at h , and θ_s is the appropriate temperature near the surface. h is determined as the first neutral level by checking the Ri_b between the lowest model level and levels above. The value of h corresponding to $Ri_{b,cr}$ is computed by linear interpolation of Ri_b at two adjacent levels. The temperature near the surface is defined as

$$\theta_s = \theta_{va} + \theta_T, \text{ where } \theta_T = a \frac{\overline{(w'\theta'_v)_0}}{w_{s0}}. \tag{7}$$

2.2. Free atmosphere diffusion

The local diffusion scheme, the so-called local- K approach (Louis, 1979) is utilized for free atmospheric diffusion above the mixed layer.

First, we compute the vertical diffusivity coefficients for momentum (m ; u , v) and scalars (t ; θ , q), following Louis (1979) above h , and these are represented by

$$K_{m,loc,t,loc} = l^2 f_{m,t}(Ri_g) \left(\frac{\partial U}{\partial z}\right) \tag{8}$$

in terms of the mixing length l , the stability functions $f_{m,t}(Ri_g)$, and the vertical wind shear, $|\partial U/\partial z|$. The stability functions $f_{m,t}$ are represented in terms of the local gradient Richardson number Ri_g .

The mixing length-scale l is given by

$$\frac{1}{l} = \frac{1}{kz} + \frac{1}{\lambda_0}, \tag{9}$$

where z is the height from the surface. Here λ_0 is the asymptotic length-scale ($=30$ m).

The YSU scheme also considers the entrainment flux above h , which expresses the penetration of entrainment flux above h irrespective of local stability. Note that the algorithm in HND06 does not contain a specific formulation for the SBL. In other words, the turbulence mixing within SBL is treated as a free atmospheric diffusion by computing the diffusion coefficients with (8–9).

2.3. The revised SBL parametrization

In the revised SBL parametrization, we keep the K -profile method as in the case of unstable situations. It is not only due to its computational efficiency, but also there is a general support for the use of K -profile similarity in parametrizations of SBL (Sharan and Gopalakrishnan, 1997; Beare *et al.*, 2006).

In the revised scheme, the vertical diffusion coefficients are computed by a prescribed parabolic shape function as in (2), but excluding the counter-gradient flux terms in (1). In (3), w_s is only a function of mechanical forcing, which is u_* . The Prandtl number in (A4) of HND06 becomes 1 because the profile functions for heat and momentum in the surface layer are identical in a stable regime ((A6) of HND06). This eliminates the height dependency. The thermal excess term in (7) is removed as well. In the determination of the SBL height, we keep the formula of (6) as in the mixed-layer diffusion, but $Ri_{b,cr}$ is greater than zero here. The study of Vickers and Mahrt (2004) is adapted to determine $Ri_{b,cr}$. By analyzing the three field program datasets, Vickers and Mahrt (2004) concluded that the best approach is to use the surface bulk Ri method with a Rossby-number-dependent critical value, $Ri_{b,cr}$, which can be expressed by,

$$Ri_{b,cr} = 0.16(10^{-7} Ro)^{-0.18}, \tag{10}$$

where Ro is the surface Rossby number, which can be expressed by

$$Ro = U_{10}/(f_0 z_0), \tag{11}$$

where U_{10} is the wind speed at 10 m from the surface, f_0 the Coriolis parameter, and z_0 the surface roughness length.

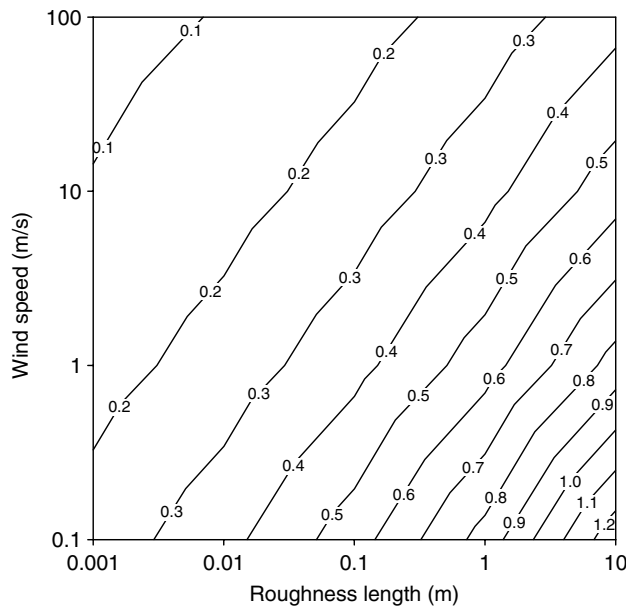


Figure 1. Computed values of the critical Richardson number as a function of the surface roughness length and 10 m wind speed (Eqs (10–11)).

f_0 is set as 10^{-4} m in this study. As seen in Figure 1, this formula allows enhanced mixing when winds are weak for a given roughness length, as compared to the $Ri_{b,cr} = 0$. Over the ocean, the $Ri_{b,cr}$ in (10–11) are applied in computing h , but it is set as a constant value greater than zero over land. This is because most land surface models use the roughness information considering the displacement heights, instead of the surface roughness length itself. Also, note that the observational evidence on the correlation between the Ro and $Ri_{b,cr}$ is not robust over land (Figure 6 of Vickers and Mahrt, 2004). Because of the lack of physical reasoning for h over land, we set it to be a theoretical value of 0.25, which is close to the value ($=0.26$) for the analysis of Cooperative Atmosphere-Surface Exchange Study CASES99 field program.

The major differences between the HND06 and revised SBL schemes include (i) the computation of PBL h using the bulk Ri greater than 0, and (ii) the parabolic profile of the eddy diffusivity coefficients with height. It is not deterministic whether the magnitude of the coefficients in the revised scheme is systematically larger than that in the HND06 since the definition is different. However, it is expected that h in the revised scheme is always greater than that from the HND06. It is noted that the revised scheme takes the mechanical mixing into account when winds are strong by reducing the computed local Ri , even if the surface buoyancy flux is negative.

Figure 2 shows that the revised SBL scheme tends to enhance mixing. This 1D offline test set-up is identical to that in HND06. The grid spacing in vertical is 20 m starting from 10 m. Of the 138 levels in the model set-up, the first six levels from the surface are shown in Figure 2. As designed above, the revised SBL scheme gradually collapses the BL, whereas the PBL height with the HND06 scheme becomes the height of the lowest model level right after sunset at 1800 local time (Figure 2(a)). A delayed collapse of the mixed layer appears for about 10 min after sunset, which is due to the residual superadiabatic layer near the surface even in the presence of negative surface buoyancy flux. With the continuous increase of downward heat flux,

the warming near the surface and cooling above the BL are distinct (Figure 2(b)), which is due to the enhanced mixing when the revised SBL algorithm is used. A comparison of the moisture profile also confirms enhanced mixing, with drying near the surface and moistening above (not shown).

In the following sections, the local Ri number scheme as described in HND06 is named the old scheme, whereas the bulk- Ri number scheme devised in this study is named the new scheme.

3. Experimental design

3.1. Model set-up

The National Centers for Environmental Prediction (NCEP) regional spectral model (RSM) is used in this study since this model has been well established for the simulation of the East Asian summer monsoon (EASM; Yhang and Hong, 2008). A model description is provided by Juang *et al.* (1997) and its application to regional climate by Hong and Leetmaa (1999). The physical processes in the RSM follow the package of Hong and Leetmaa (1999), except for using the YSU BL.

The domain covers East China, the Korean Peninsula, Japan, and the surrounding oceans (Figure 3). The map projection is the polar stereographic projection with the central longitude of 127.5°E . The number of grid points is 109 (west–east) by 86 (north–south), and a 50 km resolution is selected. The grid system has 28 vertical layers with a terrain-following sigma coordinate. The sigma values for prognostic variables for six levels from the surface are 0.995, 0.982, 0.964, 0.942, 0.915, 0.883, which resolve five layers within 1 km. The lowest model level has a sigma value of 0.995, which corresponds to about 30–50 m above the surface. We recognize that a relatively coarse resolution in the vertical could be partly responsible for the shallow PBL in the HND06 algorithm. The sensitivity of PBL schemes to the vertical resolution is an important subject to pursue in future.

The numerical experiments using the old and new SBL schemes are named the CTL and SBL experiments, respectively. Another sensitivity experiment (SBL2) with a doubled $Ri_{b,cr}$ in computing SBL height is conducted to clarify the impact of SBL mixing on the simulated precipitation and associated monsoonal circulations. Realizing that the SBL height is proportional to the value of $Ri_{b,cr}$ in (10–11), it is thus expected that the magnitude of mixing in the SBL2 run is further enhanced compared with that in the SBL run.

Before investigating the impact of SBL mixing on the EASM, the 48-hour forecasts are performed every 0000 UTC for the month of July 2006 to examine the local impact of the SBL mixing. The NCEP Final analysis (FNL) data are used for initial and boundary conditions, and also for verification of the results. The lateral boundary and base fields were linearly interpolated in time from the 6-hour FNL data. The SSTs were obtained from observation with a resolution of 1° (Reynolds and Smith, 1994). The PBL structures from the CTL and SBL experiments are further evaluated against radiosonde data. Radiosonde observation data for specific humidity and temperature are used. These data originate from the University of Wyoming website (UWYO; <http://weather.uwyo.edu/>) and are processed through a simple quality control.

The single-month regional climate run for July 2006 is designed to investigate the role of SBL mixing in modulating

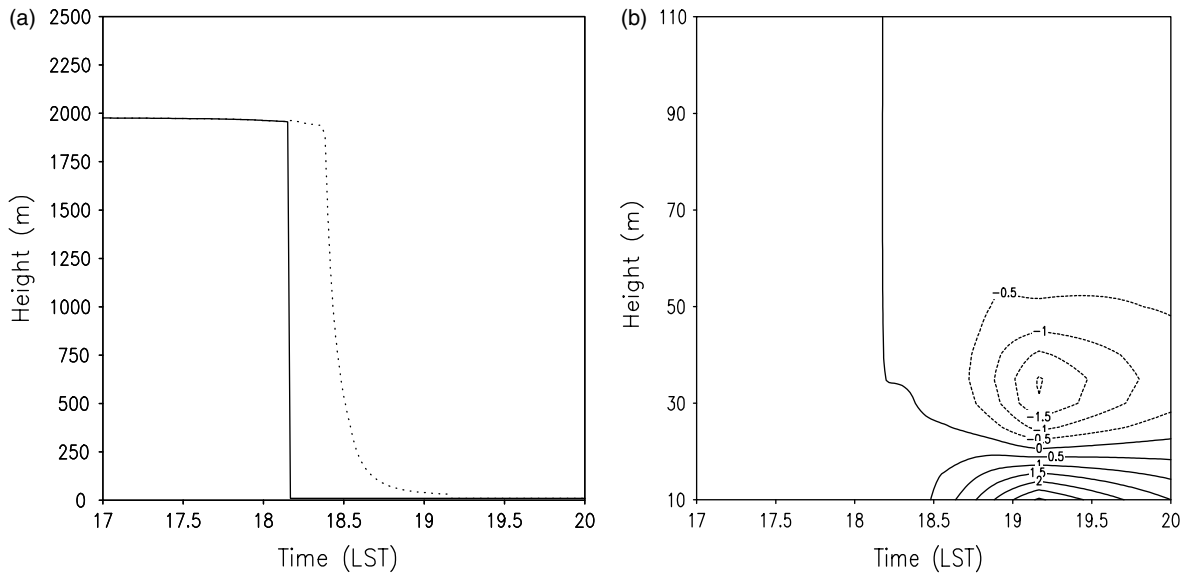


Figure 2. Time evolution of (a) the PBL height (m) obtained from the HND06 PBL (solid), and the revised SBL scheme (dotted), and (b) the differences in the potential temperature (K; revised SBL minus HND06 scheme).

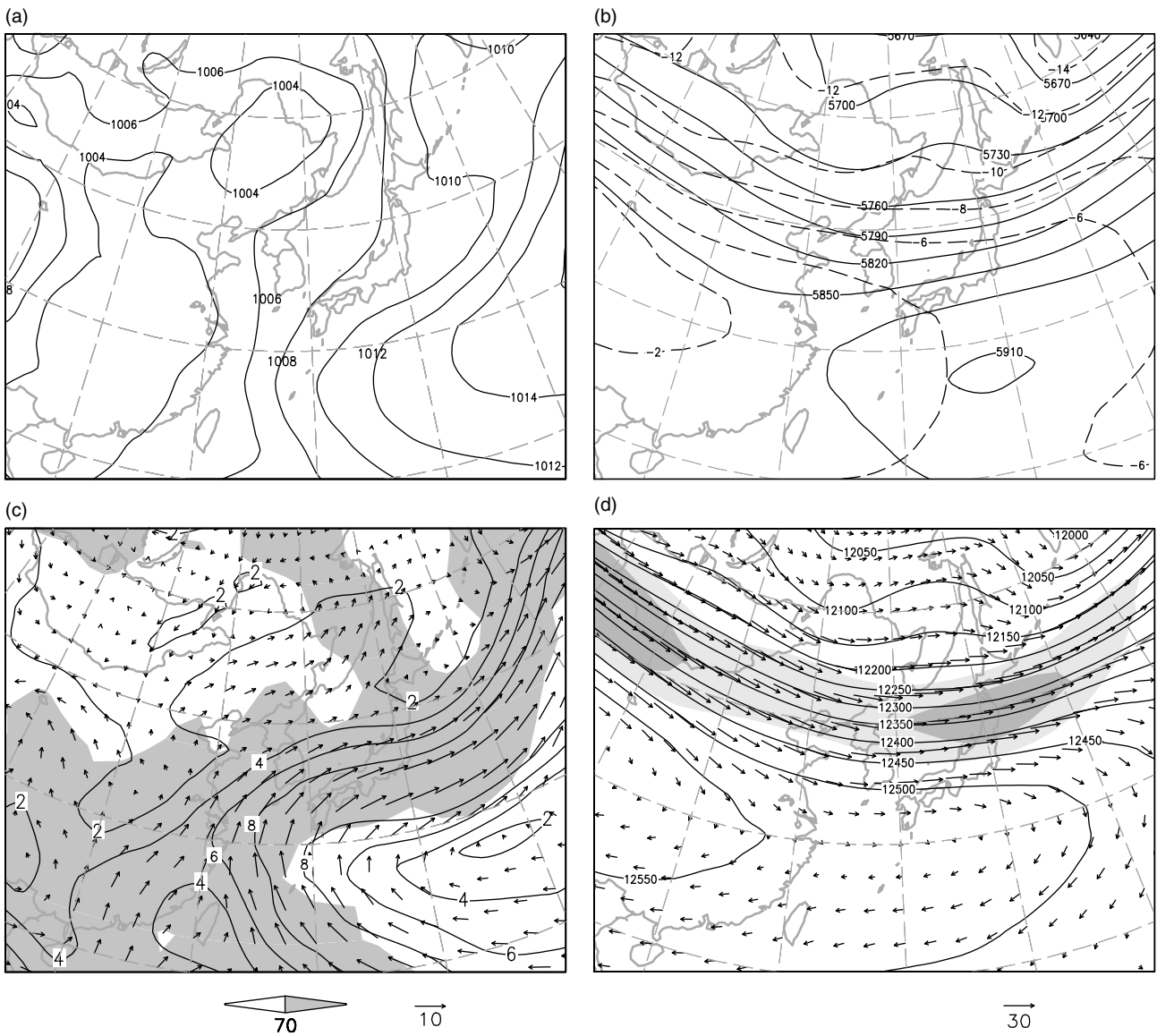


Figure 3. (a) Sea level pressure (hPa), (b) 850 hPa wind (arrows and speed contours, m s^{-1}), and relative humidity (shading $>70\%$), (c) 500 hPa geopotential height (solid contours, m) and temperature (dashed contours, K), and (d) 200 hPa wind (arrows, m s^{-1}) and geopotential height (contours, m) averaged over July 2006. In (d), shading indicates where wind speed is greater than 25 m s^{-1} (light) and 30 m s^{-1} (dark).

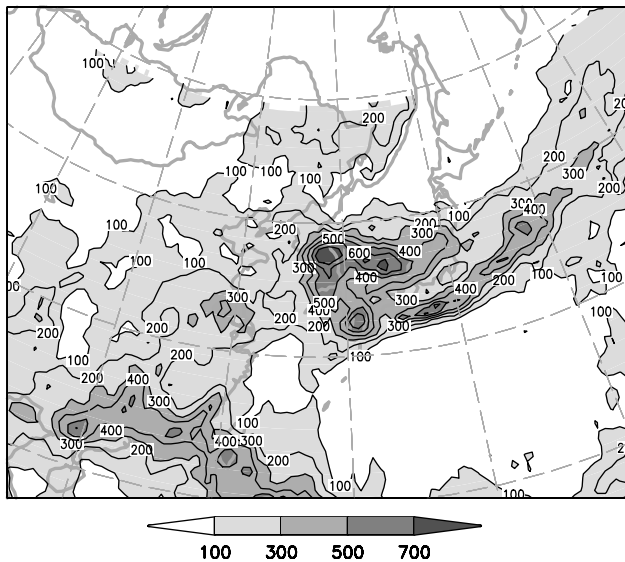


Figure 4. The monthly precipitation estimates (mm) from TMPA for July 2006. The contour interval is 100 mm.

the monsoonal precipitation, for the CTL, SBL, and SBL2 experiments. Initial conditions were obtained from the NCEP Department of Energy (DOE) reanalysis-II data (Kanamitsu *et al.*, 2002; RA2 hereafter). The lateral boundary and base fields were linearly interpolated in time from the 6-hour reanalysis data. The SSTs were updated daily from observation (Reynolds and Smith, 1994). In order to remove natural variability of the model, all experiments for July 2006 consist of three ensemble members. Each member is initialized at 0000 UTC on 29 June, 30 June, and 1 July 2006. This kind of regional climate framework can be a useful testbed in evaluating the physics parametrization since the large-scale forcing is preserved during the model integration (Ghan *et al.*, 1999). Also, it generally does not require the large number of ensemble members except for the case of soil moisture spin-up (Wang *et al.*, 2004).

The impact of SBL mixing on the simulated EASM is evaluated for 10-year summers to provide the climatological impacts. The three-month (June–July–August) seasonal run from 1999 to 2008 is designed for the CTL and SBL experiments.

The observed precipitation data set for verification of the model results is the Tropical Rainfall Measuring Mission (TRMM) Multi-satellite Precipitation Analysis (TMPA) on $0.25^\circ \times 0.25^\circ$ global grids every three hours (Huffman *et al.*, 2007).

3.2. A synoptic overview in July 2006

The typical summer over Korea is characterized by heavy rainfall, mainly connected with the Changma front in late June and July (sometimes related to typhoon activity) and a hot spell from late July to mid-August. Figure 3 shows the synoptic features averaged over July 2006, obtained from RA2. Figure 3(a) shows low sea level pressures over southern and central China, whereas a high pressure system is located over southeast Japan – a typical pressure distribution associated with a summer monsoon in July (Lee *et al.*, 1998). In the lower troposphere (Figure 3(b)), analysis shows that warm and moist air is advected from the southwest to South Korea, intensifying convection instability in that region. At 500 hPa (Figure 3(c)), a mid-level trough appears to

the west of the Korean peninsula, continuing to provide a dynamic environment favourable for inducing monsoonal rainfall. The existence of high upper-level wind speeds just to the northeast of South Korea reveals a typical synoptic feature associated with heavy rainfall over South Korea (Figure 3(d)). The one-month accumulated precipitation from the TMPA observations represents two major rain bands, one of which is over the subtropics covering South China and the southeastern China Sea, and the other in midlatitudes, where local maxima appear over Korea and Japan (Figure 4).

4. Results and discussion

4.1. Evaluation of the PBL structure (short-range forecasts)

Figure 5 shows the domain-averaged profiles of the bias and RMS error for temperature and specific humidity. The time slot for evaluation is 1200 UTC (2100 local time in Korea and Japan) and 0000 UTC (0900 local time), which correspond to 12-hour and 24-hour forecasts, respectively. We define 1200 and 0000 UTC as sunset and sunrise, respectively. The number of stations in the model domain is 113. The profiles for 1800 UTC are desirable for the evaluation of nocturnal stable mixing, but are mostly missing. Thirty days are averaged from 1 to 30 July 2006. The model output data are assigned to the station points by a simple four-point interpolation method.

For temperature, the CTL run exhibits a cooling near the surface at sunset and warming at sunrise (Figure 5(a)). Warming at 925 hPa at sunrise is about 0.5 K. The SBL run tends to warm near the surface and to cool above. Warming near the surface at sunrise does not improve the results, but overall behaviour show a decrease of the RMS errors (Figure 5(c)). The improvement for moisture is distinct (Figures 5(b,d)). Drying near the surface is prominent in the case of SBL, in particular at sunset, which reduces the bias by about 0.4 g kg^{-1} . Drying near the surface and moistening at 925 hPa at sunrise improve the bias when the new SBL scheme is introduced. At both sunrise and sunset, the revised SBL scheme reduces the RMS errors below 850 hPa (Figure 5(d)).

This local analysis confirms the appropriateness of the enhanced stable mixing designed in this study. However, this validation is limited to land at sunrise and sunset because of the lack of radiosonde observations. Thus, the evaluation of the two schemes is further extended with the FNL data, as shown in Figure 6. Over land (Figures 6(a,b)), cold and moist biases in the lower troposphere, particularly during nighttime, are largely alleviated by the enhanced mixing. The positive impact is less distinct but still visible over the oceans (Figures 6(c,d)). Compared to the radiosonde observations, the magnitude of temperature bias in the CTL run from the FNL is similar at 12 h, but opposite at 24 h (cf. Figures 5(a) and 6(a)). At 24 h (sunrise), the radiosonde verification (Figure 5(a)) for the CTL simulation reveals a warming below 925 hPa, but a cooling as much as 1 K at the surface is seen when the FNL data are used for verification (Figure 6(a)).

This indicates that the FNL data may suffer from a warm bias in the early morning, which is also alleviated by the enhanced mixing, but there is another verification issue arising from the difference in the number of verifications. Only 113 radiosonde evaluations are available,

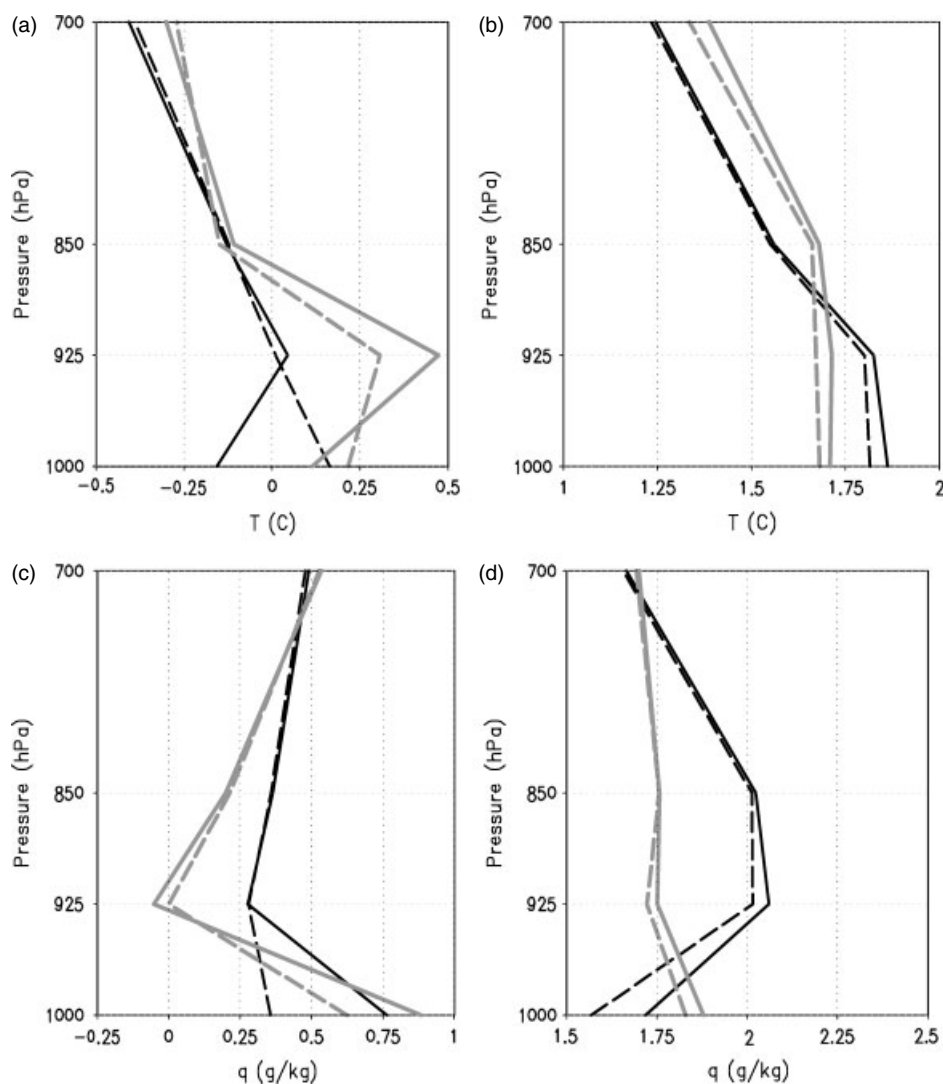


Figure 5. The biases for (a) temperature and (b) specific humidity from the CTL (solid) and SBL (dashed) experiments from radiosonde observations, and (c, d) the corresponding RMSEs. Black and grey lines denote the time at 1200 UTC (12-hour forecast) and 0000 UTC (24-hour forecast), respectively.

equivalent to about 1% of the land points in RSM. Also, most of radiosonde stations are located over Japan, Korea, and Eastern China. The enhanced mixing over the northwest mountainous regions of the model domain, where radiosonde observations are sparse, would produce a warming around 900 hPa, which in turn results in overall warming in the entire land points.

Despite some uncertainties in evaluation, it is clear that the new SBL scheme improves the PBL structure by the introduction of enhanced mixing, as originally designed and shown in the 1D test (Figure 2). We can also deduce that the PBL structure over the oceans is closer to what it should be, although *in situ* observations are not available.

4.2. Effects of the enhanced SBL mixing (July 2006)

Figure 7 compares the one-month accumulated precipitation from the model results, with the tabulated evaluation results given in Table I. In this section, only the ensemble averages of the July mean from the three experiments are shown and discussed. As seen in Table I, the ensemble spread for three-member simulations is small enough compared to the averaged amount. The TMPA data at a 4 km resolution are interpolated to the RSM grid at about 0.5° to obtain the

statistical scores in the table. The CTL run fairly well simulates excessive rainfall in the subtropics and midlatitudes compared with the observations (cf. Figures 7(a) and 4)); however, the monsoonal rainfall in central China, Korea, and Japan is displaced northwards (Figure 7(b)). Consequently, the underestimation of precipitation in Korea and Japan is distinct, whereas surplus precipitation appears in North China, Manchuria, and Siberia, which leads to the degradation of skill in simulated precipitation (Table I). The behaviour of excessive precipitation over land was found to be systematic in other regional models (Fu *et al.*, 2005; Park *et al.*, 2008).

Compared to the CTL simulation results, the SBL experiment displaces the monsoonal rainfall southwards, resulting in the increase of rainfall amounts in Central China, Korea, and Japan (Figures 7(c,d)). Enhanced mixing in the SBL2 experiment moves the monsoonal rainfall further to the south compared with the results from the CTL experiment (not shown). Consequently, the CTL surplus precipitation north of the observed is reduced in SBL. The behaviour in the new SBL experiments together with the increase of BL height in the case of the new scheme, and, as will be shown later, the further increase in the SBL2 experiment, indicate a strengthened turbulent

Table I. The amount of the ensemble average for one-month precipitation (mm day^{-1}) in July 2006, and its corresponding ensemble spread (mm day^{-1}), and the statistical skill scores, bias (mm day^{-1}), RMSE (mm day^{-1}), and spatial pattern correlation (PC) coefficients, from the CTL, SBL, and SBL2 experiments.

	Land					Oceans				
	Amount	Spread	Bias	RMSE	PC	Amount	Spread	Bias	RMSE	PC
CTL	5.91	0.94	1.29	3.86	0.62	4.84	0.77	-0.01	4.27	0.35
SBL	5.88	1.00	1.23	3.60	0.69	5.08	0.89	0.29	4.08	0.43
SBL2	5.87	1.00	1.23	3.48	0.72	5.17	0.85	0.41	4.04	0.46

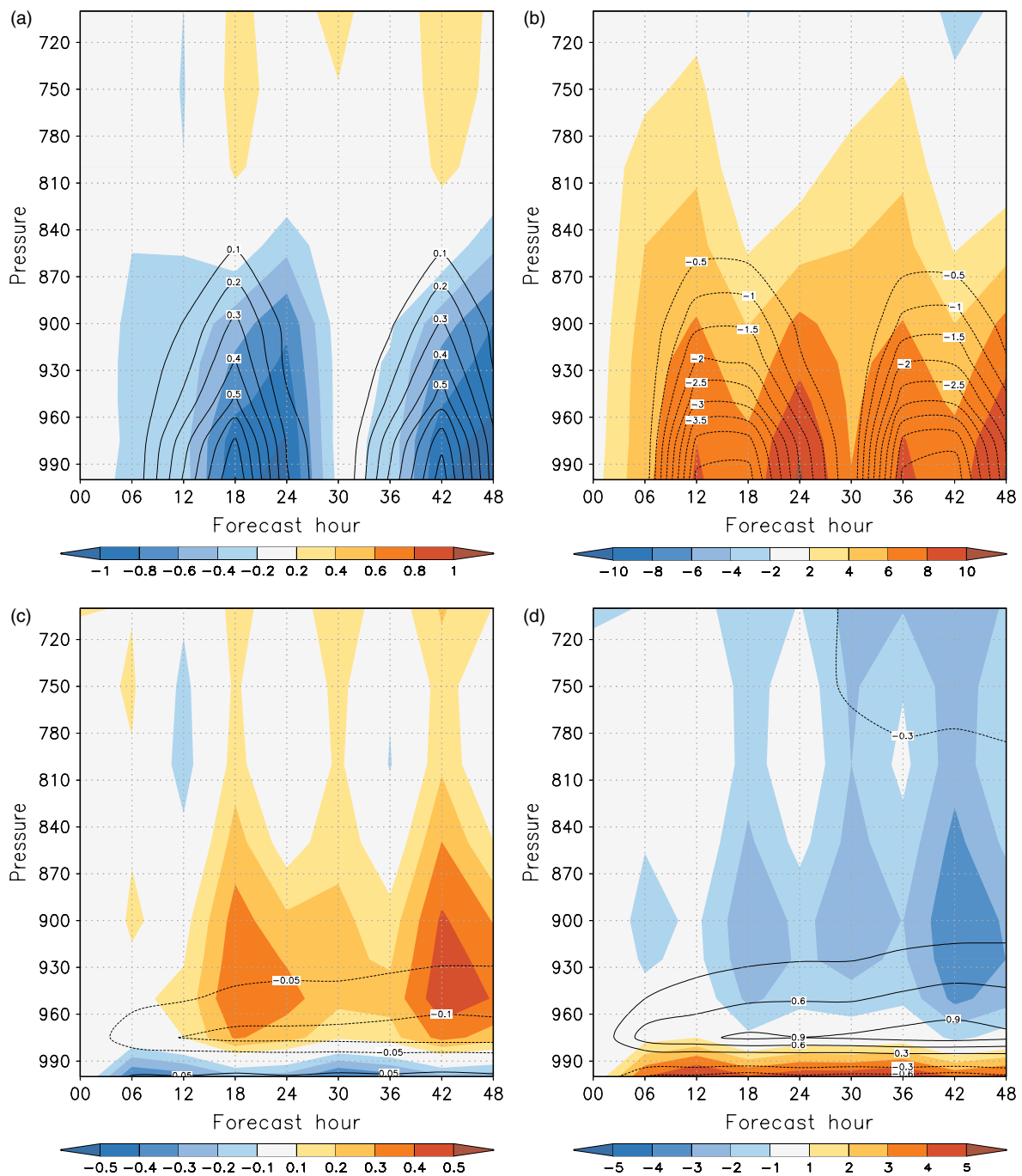


Figure 6. Time series of the vertical profiles of the differences in 29-day averaged temperature (shading, CTL minus FNL; contours, SBL minus CTL) over (a) land and (c) oceans, and (b, d) the corresponding relative humidity. Note that the contour and shading intervals for oceans are halved.

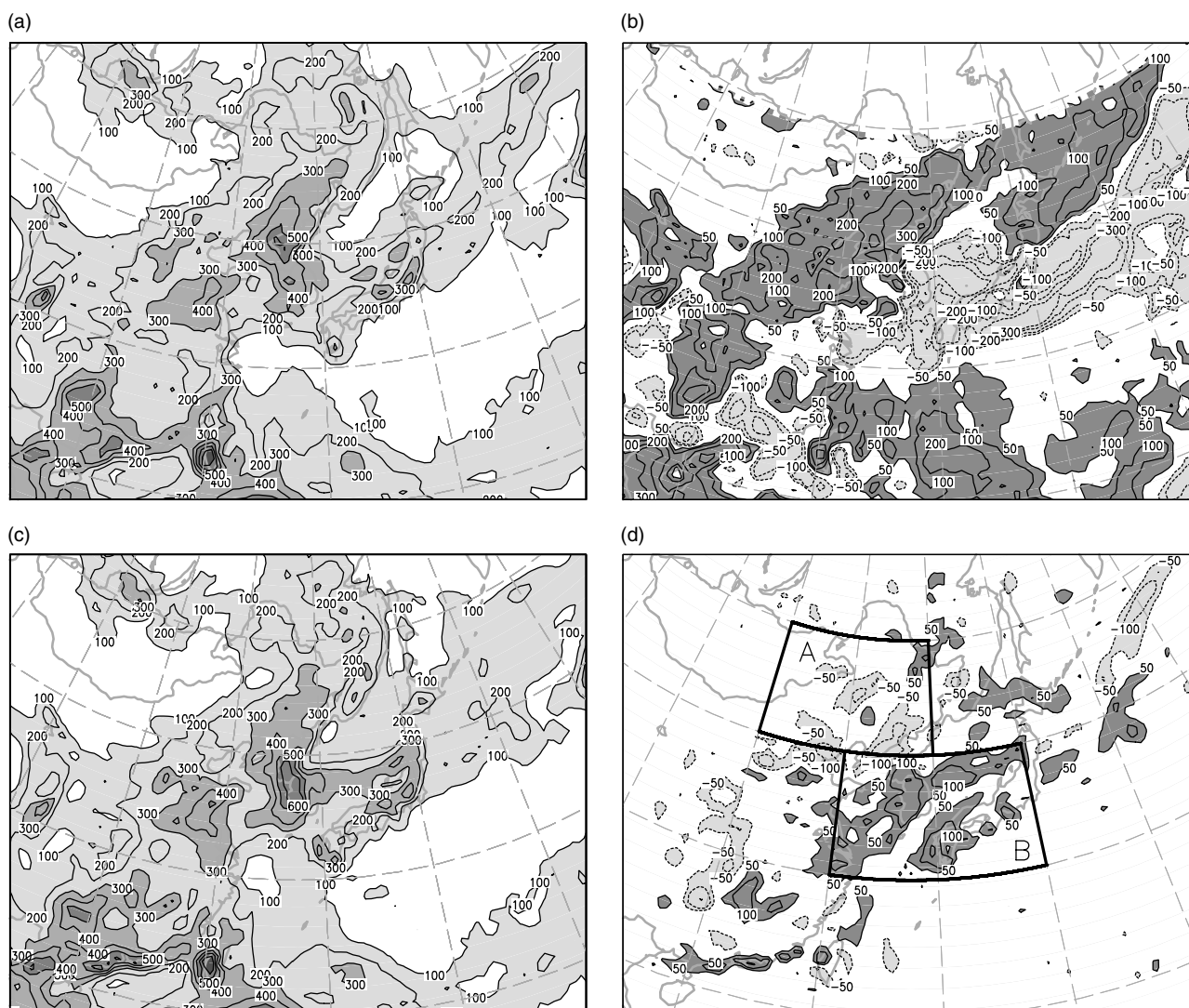


Figure 7. The monthly (July 2006) accumulated precipitation (mm) from (a) the CTL experiment and (b) the corresponding CTL minus TMPA differences (mm). (c) shows precipitation from the SBL experiment, and (d) the SBL minus CTL differences (mm). The boxes 'A' and 'B' in (d) designate the areas for the time series analyses in Figures 9 and 10.

mixing in the new scheme. Since the CTL run overestimated the precipitation amount over both land and oceans, the enhanced SBL mixing increases the bias over the oceans, whereas it is improved over land (Table I). In this table, it is seen that although the total amount of domain-averaged precipitation is further overestimated in the SBL and SBL2 experiments, the RMS errors and PC are improved, compared with those from the CTL run; this indicates an overall improvement of the precipitation patterns when the new scheme is employed.

Figure 8 shows the monthly mean fields of the BL heights and 850 hPa winds from the SBL run, and their differences from the CTL run. The distribution of the BL heights shows a maximum over the ocean to the southeast of Japan and another over the Mongolian region (Figure 8(a)). The former is related to the Pacific high and the latter is associated with high daytime sensible heat flux in the desert region. It is apparent that values are relatively low over the monsoonal precipitation region. Compared to the CTL simulation, the SBL run reveals an increase of the BL height over the whole domain (Figure 8(b)). Over land, an overall increase is pronounced, centred in North China and Manchuria, whereas its increase is distinct along the

midlatitude monsoonal precipitation regions. It is noted that areas of large BL height north of the monsoonal precipitation are correlated with reduced amounts of precipitation, whereas regions with increased BL heights roughly coincide with the enhanced precipitation activities (cf. Figures 7(d) and 8(b)). In relation to the precipitation and turbulence activities, the position of the southwesterly low-level jet (LLJ) is shifted southwards in the SBL experiment, compared with that from the CTL experiment (Figures 8(c,d)). The location of the LLJ is a critical factor in the East Asian monsoon since major precipitation occurs to the north of it where cyclonic rotation exists (Lee *et al.*, 1998)

Understanding why the SBL experiment results in an overall improvement in the simulation of monsoonal precipitation and associated large-scale circulations is not straightforward. Thus, we focus on specific regions where the impact of the enhanced SBL mixing is opposite: an area of weakened precipitation and another with enhanced precipitation activities. Region 'A' in Figure 7(d) represents the area in which the SBL run reduces the precipitation, and region 'B' denotes enhanced precipitation, both compared to the results from the CTL run. In Figure 9(a), it is apparent that precipitation in the 'A' region is reduced,

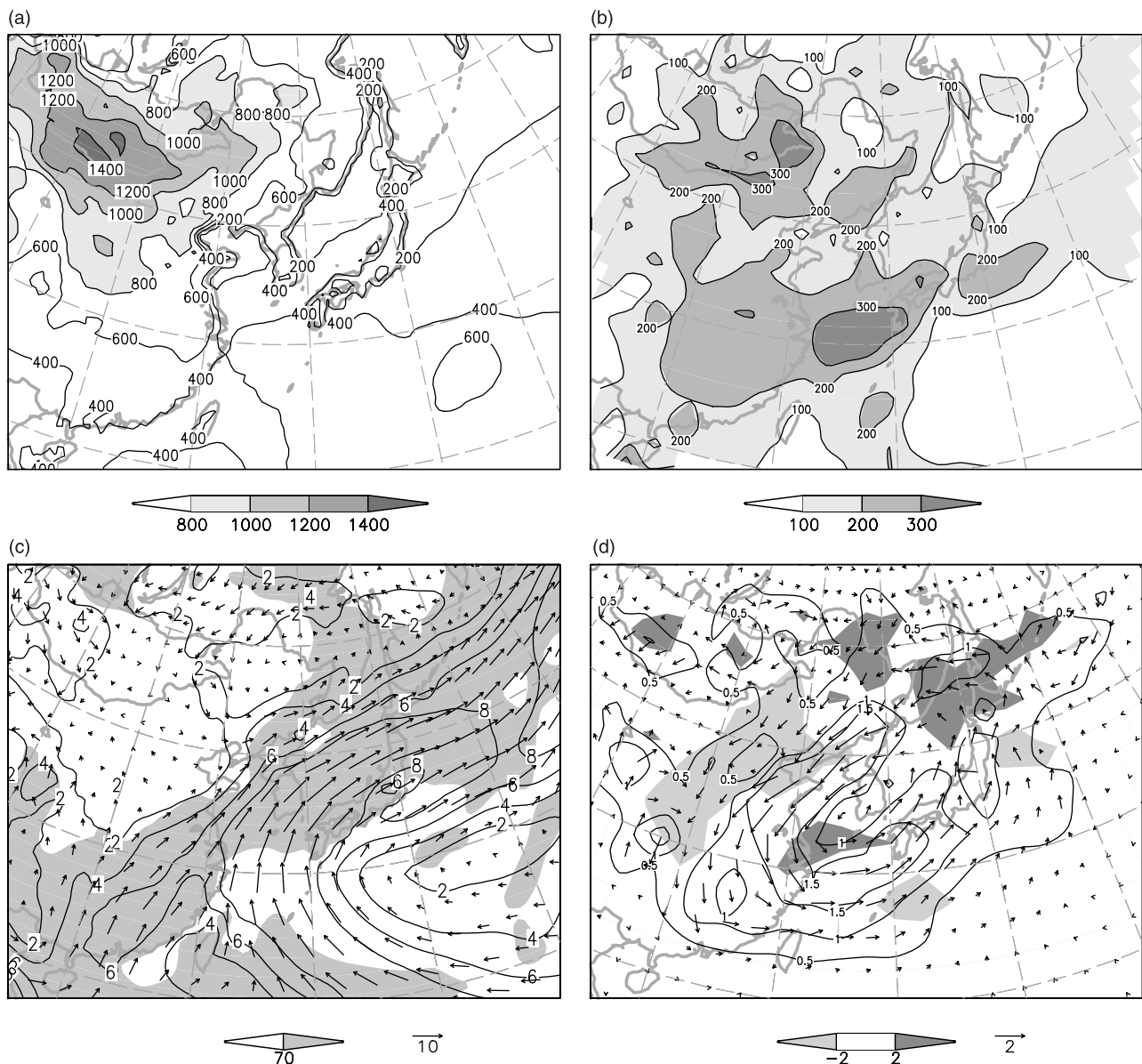


Figure 8. (a) The monthly averaged BL heights (m) from the SBL experiment, (b) the corresponding SBL minus CTL differences, (c) the SBL experiment 850hPa wind (arrows and speed contours, m s^{-1}) and relative humidity (shading $>70\%$) and (d) the corresponding SBL minus CTL differences. In (d), shading indicates an RH increase of $>2\%$ (dark) and a decrease of $>2\%$ (light).

towards what was observed, as the mixing is enhanced. The reduction of precipitation is distinct not only during nighttime (0900–2100 UTC), but also in daytime. As expected, the BL height increases as the mixing is enhanced, in particular at night (Figure 9(c)). The increase in BL height (Figure 9(d)) is similar at night in regions 'A' and 'B', the point is that in region 'B' it occurs in the daytime too. In contrast to the features in region 'A', the precipitation amount decreases as the SBL mixing is strengthened (Figure 9(b)).

The impact of the SBL mixing on the resulting large-scale circulation is better seen in the vertical profiles of temperature and moisture (Figure 10). It is seen that the CTL run produces a warm bias over the RA2 data except for the upper troposphere. For region 'A', the direct impact of the enhanced mixing appears at night accompanying a weak warming peak at 1200 UTC near the surface (Figure 10(a)). Above the warming region, compensating cooling appears, which alleviates the bias in the CTL run. Above 200 hPa, the cold bias in the CTL run is also greatly reduced in

the case of the SBL run. The bias reduction in the upper troposphere can be attributed to the suppressed precipitating convection when enhanced mixing is introduced. Because of the reduced upper clouds, long-wave heating below the clouds and cooling above are reduced toward what was observed. This scenario largely complies with the analysis of the cloud–radiation feedback in a simulated precipitating convection over Korea (Figures 12 and 13 of Hong *et al.*, 2004, and the related discussions therein). The SBL run decreases the moist bias near the surface at night, and layers around 550–700 hPa and 100–200 hPa, but increases the bias above the BL and layer around 300 hPa (Figure 10(b)). The moisture bias in the CTL run and impact of the SBL mixing are not as systematic as in the case of temperature, which can be due to the complicated interaction with precipitation and moisture.

As in the case of region 'A' in the CTL run, region 'B' experiences similar behaviour in terms of the warm bias within most of the troposphere. For temperature

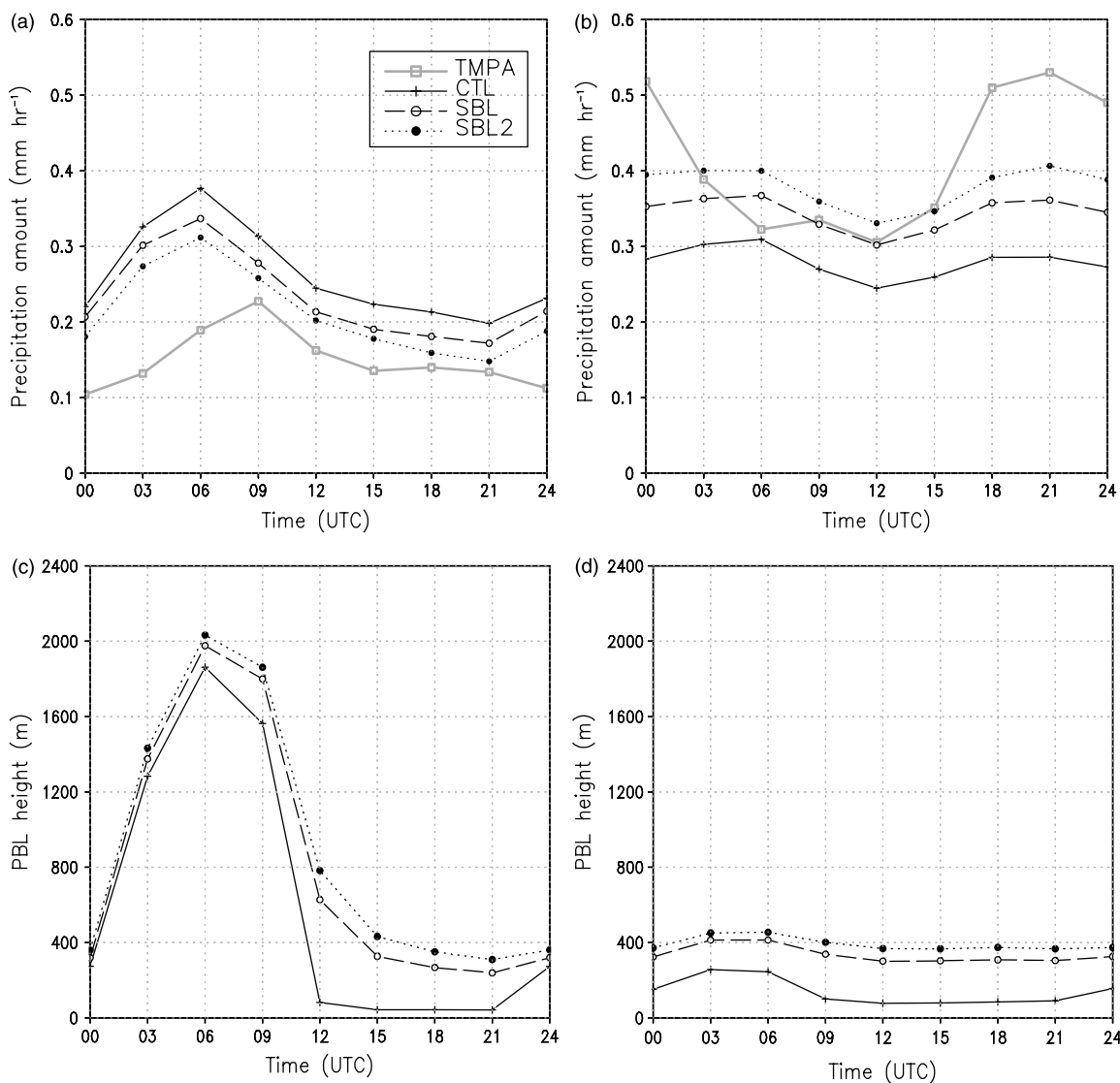


Figure 9. Diurnal variations of the monthly averaged precipitation in (a) region 'A' and (b) region 'B', with (c, d) the corresponding BL heights. Regions 'A' and 'B' are marked in Figure 4(d).

(Figure 10(c)), the SBL experiment reduces the warm bias in the lower troposphere, although the amount of the correction is not large enough to compensate for the bias in the CTL run. Warming above 300 hPa by the SBL run indicates enhanced precipitating convection. The bias of the CTL run and its correction by the SBL run are more systematic for moisture than for temperature (Figure 10(d)). Drying peaks at 900 hPa and above are greatly reduced by the incorporation of the new SBL mixing. Moistening above 300 hPa in the CTL run is remarkably reduced in the SBL run. In the upper troposphere, the changes in temperature are opposite between the regions 'A' and 'B', since the response of the precipitation due to enhanced SBL mixing is opposite. In other words, the changes in temperature and moisture in the upper troposphere are the indirect effect of the SBL mixing through the interaction with the precipitation processes.

4.3. Further discussion on the interaction between the SBL and precipitation

A more robust evaluation of the changes in the large-scale circulations will be made in the next subsection,

but it is critical to clarify the reason for the different precipitation response by the new SBL mixing. The BL height is greater as the SBL mixing is stronger in both regions. A major difference is the height of BL and the humidity: the relative humidity (RH) is higher in region 'B' than in region 'A' (Figure 8(c)). In region 'A', the height of the BL experiences typical daytime free convection and nocturnal BL mixing over land, which intimately interacts with the diurnal variation of the surface fluxes. In this situation, reduced cooling and moistening near the surface at night induces a less favourable environment to trigger precipitating convection, since the air is relatively dry. The decrease of the daytime precipitation can be attributed to a remaining effect of the enhanced SBL mixing in the morning accompanying a less stable structure. Thus, the weakened precipitating activities can be due to raising the lifting condensation level in a relatively dry region (Figure 10(b)).

On the other hand, in region 'B' the BL is relatively moist and does not experience a feedback from the surface since the SST is not altered by the atmosphere. In this situation, the enhanced mixing in the SBL run plays a role in moistening and cooling the PBL top, which leads to a favourable environmental condition to trigger

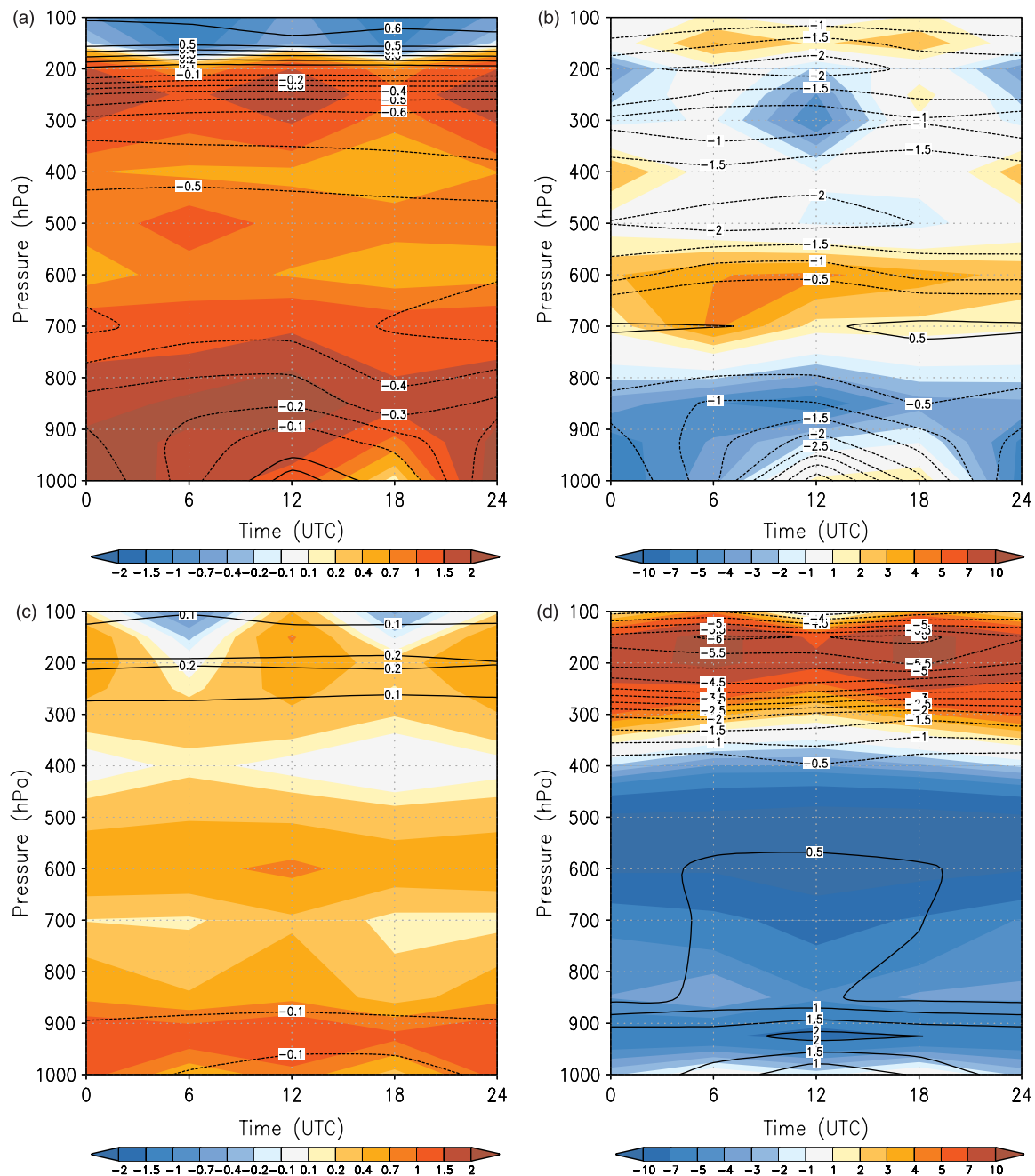


Figure 10. Diurnal variations of the vertical profiles of the differences in monthly domain-averaged temperature (shading, CTL minus RA2; contours, SBL minus CTL) over the regions (a) 'A' and (c) 'B', and (b, d) the corresponding relative humidity.

precipitating convection. Changes in RH by the new SBL mixing demonstrate these scenarios in the subcloud layer. RH at the PBL top in a stable regime, which is around 950 hPa, is decreased in region 'A' (Figure 10(c)), whereas it is increased in region 'B' (Figure 10(d)). In contrast to the land points, over the oceans the surface boundary condition represented by the SST is well known to play a major role in forcing the atmosphere, and understanding its role has been a simpler task, both because SST is observed daily and because the surface is saturated at this temperature. For this reason, the enhanced BL mixing over water can enhance the precipitation activities. A comprehensive description of the surface layer–atmosphere interaction over land and water is available in Betts *et al.* (1996).

Finally, the rainfall changes should be related to large-scale circulation changes in addition to local responses. It is

believed that the southward shift of the LLJ in Figure 8(d) is balanced with the changes in precipitation due to the enhanced SBL mixing. One can see that the cyclonic rotation is increased to the south of the LLJ, where the precipitation activity is enhanced (region 'B'), whereas it is decreased where the anticyclonic rotation is increased (region 'A'). The enhanced cyclonic circulation in region 'B' induces the moistening throughout the convergence, which can increase the humidity in region 'B' (Figure 10(d)), but it is difficult to isolate the local effect and large-scale-induced remote feedback in this 3D monthly climatology. Realizing that the enhanced SBL produces a warming and drying in non-precipitation conditions, as documented in this study, the cooling and moistening over the ocean surface could be due to the dominant dynamical effects accompanying strengthened moisture convergence, together with enhanced

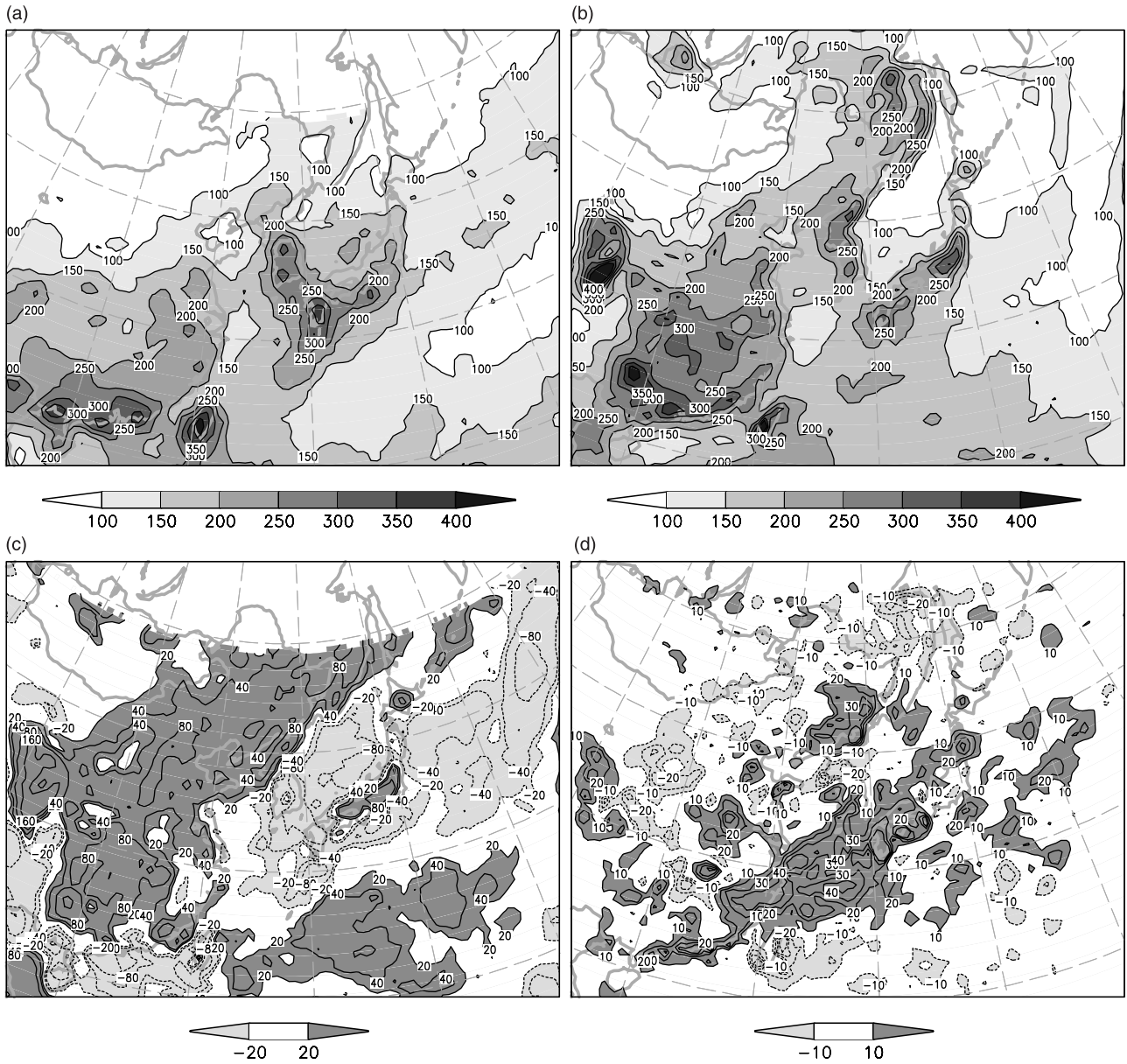


Figure 11. (a) Monthly precipitation estimate (mm) from TMPA for the 10-year mean summer (JJA) precipitation (mm month⁻¹) from 1999 to 2008. The contour interval is 50 mm above 100 mm. (b) is the corresponding estimate from the CTL experiment (with a land/ocean pattern correlation of 0.82/0.65). (c) shows CTL minus TMPA (with land/ocean bias of 31.95/−4.37 mm, and contours at ±160, ±80, ±40, ±20), and (d) SBL minus CTL (with land/ocean biases of 2.19/2.31 mm, and contours at ±40, ±30, ±20, ±10).

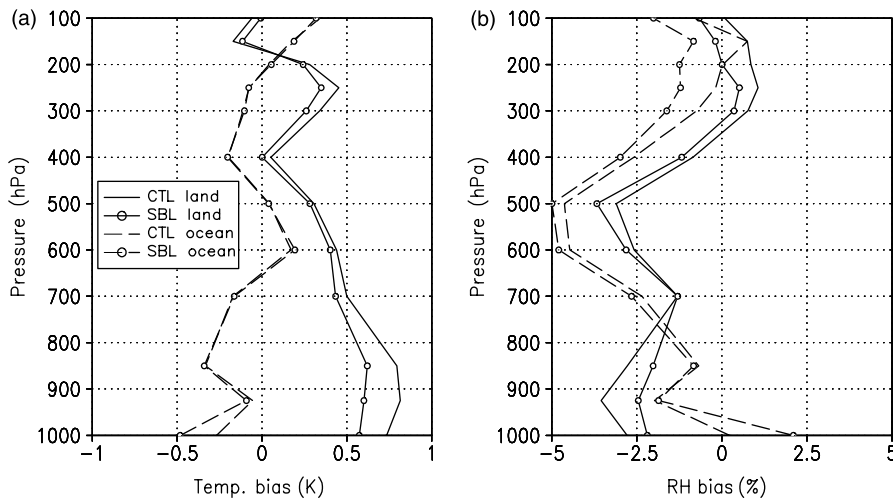


Figure 12. The vertical profiles of the biases in (a) temperature and (b) relative humidity (RH), averaged over the domain over the 10-year simulation period.

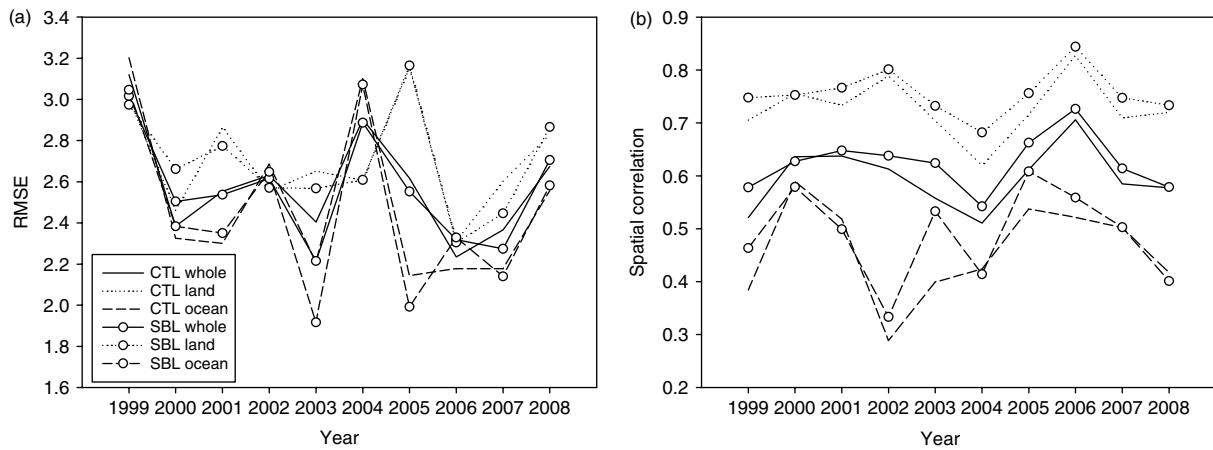


Figure 13. The time series of (a) RMSE (mm day^{-1}) and (b) spatial pattern correlation, for JJA precipitation from 1999 to 2008.

precipitation inducing evaporation of raindrops near the surface.

4.4. Impacts on the simulated climatology (1999–2008)

In this section, results from the 10-year-averaged summer simulations from the CTL and SBL runs are compared. The impacts of the revised SBL effects on the distribution of precipitation and large-scale features for summer qualitatively follow those from the 1-month run discussed in the previous section, as will be discussed below.

The 10-year-averaged JJA precipitation for TMPA data represents the monsoonal rain band extending northeastwards from southern China to the northern part of Japan (Figure 8(a)). Reflecting the similarity in the distribution of precipitation between the 10-year summer and July 2006 (cf. Figures 4 and 11(a)), the 10-year summer climatology of the large-scale circulation qualitatively followed the subtropical high over the northwestern Pacific and midlatitude East Asian trough, elongated northeastwards from east China to Manchuria (cf. Figure 4(b)).

It is seen that the CTL experiment reproduce the precipitation centre over southern China, Korea and Japan fairly well (Figure 11(b)). However, excessive precipitation over the subtropics and most of China is prominent, whereas a deficit in the amount of precipitation occurs in the central region of the monsoon band, near Korea and Japan (Figure 11(c)). These bias patterns were identified in the 1-month simulation (Figure 7(b)). The SBL experiment tends to reduce the bias over the monsoonal precipitation region by increasing the precipitation amount (Figure 11(d)). An increase of precipitation in central China near 30°N causes the climatology to deteriorate, but Table II shows that the overall skill for monsoonal precipitation in the SBL experiment is better than in the CTL run. It was seen that the LLJ from southeastern China and subtropical oceans is exaggerated by the CTL run, which is associated with the overestimation of precipitation in north China and its underestimation near Korea and Japan (not shown). The SBL run was found to decrease cyclonic circulation in northern China and its increase to the southeast of the LLJ, as in July 2006 (Figure 8(d)). These changes in the lower-tropospheric circulation play a role in enhancing the oceanic precipitation (Table II).

The vertical profiles of the biases in temperature and moisture over the RA2 are shown in Figure 12. The profiles of the RMSE (not shown) followed the bias distributions. The domain-averaged temperature bias shows a warm bias over land, with the distinct reduction of warm bias in the lower troposphere when the enhanced SBL mixing is introduced. A cold bias appears over the oceans decreasing upwards, which is not affected by the SBL experiment. A further cooling exists near the surface in the case of the SBL run. The impact of the enhanced SBL mixing on the RH profiles is mixed. Except for a distinct reduction of dry bias below 700 hPa over land, the SBL run tends to slightly deteriorate the bias magnitude. This mixed effect of the SBL mixing in the RH profiles can be attributed to the influence of the modified BL structure on the resulting precipitation activities and subsequent feedback to the large scales.

Figure 13 compares the interannual variation of RMSE and pattern correlation for seasonal precipitation over 10 years, obtained from the CTL and SBL experiments. It is seen that the RSME values experience a distinct interannual variation (Figure 13(a)). The skill is relatively low in 1999, 2004, and 2008, whereas the seasonal precipitation is well reproduced in 2000, 2001, 2003, and 2005. A relatively distinct improvement is found for oceanic rainfall in 2003 and 2005 summers by the SBL experiment. The overall impact reveals that the RMS errors are not influenced by the SBL, whereas there is a fairly consistent improvement in the pattern correlation (Figure 13(b) and Table II), which reflects the improved distribution but also the remaining bias. Table II demonstrates that the pattern correlation is noticeably better over land than ocean in both model experiments, while the RMS errors and biases are larger. From these results, it can be said that the inclusion of the revised SBL processes designed in this study effectively improves the monsoon climatology.

5. Concluding remarks

In this study, we designed a new SBL scheme, based on the bulk Richardson number between the surface layer and the top of the BL and implemented in the Yonsei University (YSU) BL scheme, which was evaluated against the local scheme in which the mixing coefficient is a function of the local Richardson number at a given model level.

A statistical evaluation of a series of 48-hour forecasts every 0000 UTC for July 2006 confirms that the BL

Table II. Statistical skill scores, bias (mm day⁻¹), RMSE (mm day⁻¹), and spatial pattern correlation (PC) coefficients, from the CTL and SBL experiments, for the ten-year climatology (1999–2008).

	Whole			Land			Oceans		
	Bias	RMSE	PC	Bias	RMSE	PC	Bias	RMSE	PC
CTL	0.40	1.79	0.74	1.09	2.17	0.82	-0.18	1.39	0.65
SBL	0.50	1.78	0.77	1.18	2.22	0.84	-0.07	1.31	0.69

structure is closer to the radiosonde observation and NCEP FNL data when the new SBL scheme is used. On a regional climate framework for July 2006, the results with the new SBL scheme demonstrate that modulating the subcloud structure with enhanced vertical mixing improves the simulated monsoon climatology by displacing the monsoonal precipitation southwards. The northward displacement of simulated precipitation over East Asia in summer has been a systematic error in other regional climate models (Fu *et al.*, 2005; Park *et al.*, 2008). Some studies focused on the convective parametrization scheme to resolve this issue, but these biases remained unchanged irrespective of the selected schemes (Kang and Hong, 2008). Our study demonstrates that, together with the local effects of the enhanced SBL mixing that warms and dries the BL, the dynamical feedbacks accompanying strengthened moisture convergence results in enhanced precipitation southwards toward what was observed. A 10-member ensemble of three-month June–July–August (JJA) simulations for 1999–2008 shows that the revised SBL scheme improves the temperature and moisture profiles in the lower troposphere, as well as the precipitation climatology. The interannual variation of seasonal precipitation is more realistic over both land and oceans.

We recognize that the algorithm for SBL proposed in this study is not the best way to represent the SBL structure in reality, and that the impact may be different using other diffusion schemes and models. Also, this scheme is relatively simple compared with other sophisticated approaches (e.g. Sukoriansky *et al.*, 2005). Despite its simplicity, as shown in this study, the interaction of the BL structure with the precipitation and associated large-scale circulations is rather complicated. The increase in mixing relative to that in the control was clearly beneficial, but further work is certainly required to compare the new scheme to other schemes, both in terms of local performance and large-scale impact (Beare *et al.*, 2006; Brown *et al.*, 2008).

Our study further suggests that care should be taken in interpreting the results of the vertical diffusion package with some modifications, since the BL structure significantly influences the simulated climate through interaction with other physical processes in weather and climate models, which is important for further improvement of existing schemes and developing a new parametrization method. In relation to this issue, Kim and Hong (2009) confirmed that the new SBL scheme designed in this study plays a critical role in representing proper interaction between the BL and gravity-wave drag processes in a version of the NCEP global model, which leads to a significant improvement of seasonal climatology of zonal wind and temperature.

Acknowledgements

This research was supported by the Basic Science Research Program through the National Research Foundation of Korea (NRF), funded by the Ministry of Education, Science and Technology (2010-0000840). The author is sincerely grateful to Si-Wan Kim for pointing out the stable boundary mixing issue in the YSU scheme, and exchanging information during the scheme development, and to Jimmy Dudhia for testing the new scheme in the WRF model. The author appreciates the work of Myung-Seo Koo, who helped in plotting some figures. Much of the work in this study was accomplished while the author visited the Scripps Institute of Oceanography as a visiting scholar, and a long-term discussion with Masao Kanamitsu should be acknowledged.

References

- Basu S, Iyengar GR, Mitra AK 2002. Impact of a non-local closure scheme in a simulation of a monsoon system over India. *Mon. Weather Rev.* **130**: 161–170.
- Beare RJ, Macvean MK, Holtslag AAM, Cuxart J, Esau I, Golaz JC, Jimenez MA, Khairoutdinov M, Kosovic B, Lewellen D, Lund TS, Lundquist JK, McCabe A, Moene AF, Noh Y, Raasch S, Sullivan P 2006. An intercomparison of large-eddy simulations of the stable boundary layer. *Boundary-Layer Meteorol.* **118**: 247–272.
- Betts AK, Ball JH, Beljaars ACM, Miller MJ, Viterbo PA 1996. The land surface–atmospheric interaction: A review based on observational and global modeling perspectives. *J. Geophys. Res.* **101**: 7209–7225.
- Braun SA, Tao WK 2000. Sensitivity of high-resolution simulations of hurricane Bob (1991) to planetary boundary-layer parameterizations. *Mon. Weather Rev.* **128**: 3941–3961.
- Brown AR, Beare RJ, Edwards JM, Lock AP, Keogh SJ, Milton SF, Walters DN 2008. Upgrades to the boundary-layer scheme in the Met Office numerical weather prediction model. *Boundary-Layer Meteorol.* **128**: 117–132.
- Bright DR, Mullen SL 2002. The sensitivity of the numerical simulation of the southwest monsoon boundary layer to the choice of PBL turbulence parameterization in MM5. *Weather Forecasting* **17**: 99–114.
- Byun YH, Hong SY 2004. Impact of boundary-layer processes on simulated tropical rainfall. *J. Climate* **17**: 4032–4044.
- Cha DH., Lee DK, Hong SY 2008. Impact of boundary layer processes on seasonal simulation of the East Asian summer monsoon using a Regional Climate Model. *Meteorol. Atmos. Phys.* **100**: 53–72.
- Davis C, Bosart LF 2002. Numerical Simulations of the Genesis of Hurricane Diana (1984). Part II: Sensitivity of Track and Intensity Prediction. *Mon. Weather Rev.* **130**: 1100–1124.
- Fu FB, Wang S, Xiong Z, Gutowski WJ, Lee D-K, McGregor JL, Sato Y, Kato H, Kim J-W, Suh M-S 2005. Regional climate model intercomparison project for Asia. *Bull. Amer. Meteorol. Soc.* **86**: 257–266.
- Ghan SJ, Leung LR, McCaa J 1999. A comparison of three different modeling strategies for evaluating cloud and radiation parameterizations. *Mon. Weather Rev.* **127**: 1967–1984.
- Holtslag AAM, Boville BA 1993. Local versus nonlocal boundary-layer diffusion in a global climate model. *J. Climate* **6**: 1825–1842.
- Hong SY, Leetmaa A 1999. An evaluation of the NCEP RSM for regional climate modeling. *J. Climate* **12**: 592–609.
- Hong SY, Pan HL 1996. Nonlocal boundary layer vertical diffusion in a medium-range forecast model. *Mon. Weather Rev.* **124**: 2322–2339.

- Hong SY, Dudhia J, Chen SH 2004. A revised approach to ice-microphysical processes for the bulk parameterization of clouds and precipitation. *Mon. Weather Rev.* **132**: 103–120.
- Hong SY, Noh Y, Dudhia J 2006. A new vertical diffusion package with an explicit treatment of entrainment processes. *Mon. Weather Rev.* **134**: 2318–2341.
- Huffman GJ, Adler RF, Bolvin DT, Gu G, Nelkin EJ, Bowman KP, Hong Y, Stocker EF, Wolff DB 2007. The TRMM multisatellite precipitation analysis (TMPA): quasi-global, multiyear, combined-sensor precipitation estimates at fine scales. *J. Hydrometeorol.* **8**: 38–55.
- Janjić ZI 1990. The step mountain eta coordinate: Physical package. *Mon. Weather Rev.* **118**: 1561–1575.
- Juang HMH, Hong SY, Kanamitsu M 1997. The NCEP regional spectral model: An update. *Bull. Amer. Meteorol. Soc.* **78**: 2125–2143.
- Kang HS, Hong SY 2008. Sensitivity of the simulated east Asian summer monsoon to four convective parameterization schemes in a regional climate model. *J. Geophys. Res.* **113**: D15119, DOI: 10.1029/2007JD009692.
- Kanamitsu M, Ebisuzaki W, Woollen J, Yang SK, Hnilo JJ, Fiorino M, Potter GL 2002. NCEP-DOE AMIP-II Reanalysis (R-2). *Bull. Amer. Meteorol. Soc.* **83**: 1631–1643.
- Kim YJ, Hong SY 2009. Interaction between the orography-induced gravity wave drag and boundary layer processes in a global atmospheric model. *Geophys. Res. Lett.* **36**: L12809, DOI: 10.1029/2008GL037146.
- Kim SW, McKeen S, Frost G, Hsie EY, Trainer M, Grell G, Peckham S 2006. 'The sensitivity of ozone and its precursors to PBL transport parameterizations within the WRF-Chem model'. In *Proceedings of 7th WRF Users' Workshop*, Boulder, Colorado, 19–22 June. Available from <http://wrf-model.org>.
- Lee DK, Kim HR, Hong SY 1998. Heavy rainfall over Korea during 1980–1990. *Korean J. Atmos. Sci.* **1**: 32–50.
- Lee SM, Giori W, Princevac M, Fernando HJS 2006. Implementation of a stable PBL turbulence parameterization for the mesoscale model MM5: Nocturnal flow in complex terrain. *Boundary-Layer Meteorol.* **119**: 109–134.
- Li X, Pu Z 2008. Sensitivity of numerical simulation of early rapid intensification of hurricane *Emily* (2005) to cloud microphysical and planetary boundary-layer parameterizations. *Mon. Weather Rev.* **136**: 3819–4838.
- Louis JF 1979. A parametric model of vertical eddy fluxes in the atmosphere. *Boundary-Layer Meteorol.* **17**: 187–202.
- Mahrt L, Sun J, Blumen W, Delany T, Oncley S 1999. Nocturnal boundary-layer regimes. *Boundary-Layer Meteorol.* **88**: 255–278.
- Martin GM, Bush MR, Brown AR, Lock AP, Smith RNB 2000. A new boundary-layer mixing scheme. Part II: Tests in climate and mesoscale models. *Mon. Weather Rev.* **128**: 3200–3217.
- Noh Y, Cheon WG, Hong SY, Raasch S 2003. Improvement of the K-profile model for the planetary boundary layer based on large-eddy simulation data. *Boundary-Layer Meteorol.* **107**: 401–427.
- Park EH, Hong SY, Kang HS 2008. Characteristics of an East-Asian summer monsoon climatology simulated by the RegCM3. *Meteorol. Atmos. Phys.* **100**: 139–158.
- Reynolds RW, Smith TM 1994. Improved global sea surface temperature analyses using optimum interpolation. *J. Climate* **7**: 929–948.
- Skamarock WC, Klemp JB, Dudhia J, Gill DO, Barker DM, Duda MG, Huang XU, Wang W, Powers JG 2008. 'A description of the Advanced Research WRF version 3'. Tech. Note NCAR/TN-475+STR. NCAR: Boulder, USA. Available from <http://wrf-model.org>.
- Sharan M, Gopalakrishnan SG 1997. Comparative evaluation of eddy exchange coefficients for strong and weak wind stable boundary layer modeling. *J. Appl. Meteorol.* **3**: 545–559.
- Shin SH, Ha KJ 2007. Effects of spatial and temporal variations in PBL depth on a GCM. *J. Climate* **20**: 4717–4732.
- Steenefeldt GJ, Mauritsen T, De Bruijn EIF, Vilà-Guerau de Arellano J, Svensson G, Holtslag AAM 2008. Evaluation of limited-area models for the representation of the diurnal cycle and contrasting nights in CASES-99. *J. Appl. Meteorol.* **47**: 869–887.
- Sukoriansky S, Galperin B, Perov V 2005. Application of a new spectral theory of stably stratified turbulence to the atmospheric boundary layer over sea ice. *Boundary-Layer Meteorol.* **117**: 231–257.
- Terra R, Mechoso CR, Arakawa A 2004. Impact of orographically induced spatial variability in PBL stratiform clouds on climate simulations. *J. Climate* **17**: 276–293.
- Troen I, Mahrt L 1986. A simple model of the atmospheric boundary layer sensitivity to surface evaporation. *Boundary-Layer Meteorol.* **37**: 129–148.
- Vickers D, Mahrt L 2004. Evaluating formulations of stable boundary-layer height. *J. Appl. Meteorol.* **43**: 1736–1749.
- Wang Y, Leung LR, McGregor JL, Lee DK, Wang WC, Ding Y, Kimura F 2004. Regional climate modeling: Progress, challenges and prospects. *J. Meteorol. Soc. Japan* **82**: 1599–1628.
- Yhang YB, Hong SY 2008. Improved physical processes in a regional climate model and their impact on the simulated summer monsoon circulations over East Asia. *J. Climate* **21**: 963–979.